JOURNAL OF SPACECRAFT AND ROCKETS
Vol. 48, No. 2, March–April 2011

Parametric Study of Dual-Expander Aerospike Nozzle Upper-Stage Rocket Engine

J. Simmons* and Richard Branam†
Air Force Institute of Technology, Wright-Patterson Air Force Base, Ohio 45433

DOI: 10.2514/1.51534

The Air Force Institute of Technology is studying a new upper-stage rocket engine architecture: the dual-expander aerospike nozzle. The goal of this research is to provide the maximum thrust-to-weight ratio in an engine that delivers a minimum of 50,000 lbf vacuum thrust with a vacuum specific impulse of 464 s. Previous work focused on developing an initial design to demonstrate the feasibility of the dual-expander aerospike nozzle architecture. That work culminated in a design exceeding the requirements, delivering an estimated 57,000 lbf thrust with a specific impulse of 472 s by using an oxidizer-to-fuel ratio of 7.03, a total mass flow of 121 lbm/s, and an engine length of 38 in. These results were computed in a numerical model of the engine. Current work expands the model in preparation for optimizing its thrust-to-weight ratio. The changes to the model are designed to support running automated parametric and optimization studies. Parametric studies varying oxidizer-to-fuel ratio, total mass flow, and chamber length show that a dual-expander aerospike nozzle engine can achieve 50,000 lbf vacuum thrust and 489 s vacuum I_{sp} with an oxidizer-to-fuel ratio of six, a total mass flow of 104 lbm/s (a reduction of 14%), and an engine length of 27.9 in. (a reduction of over 25%), which should equate to a significant weight savings over the original design.

Nomenclature

a = half spacing of channel, in.
$A_{cv,i}$ = cross-sectional area of cooling volume at ith station, in.^{2}
$A_{flow,i}$ = combusted flow cross-sectional area at ith station, in.^{2}
A_{hx} = area of heat exchange for chamber, in.^{2}
$A_{hx_{cv,i}}$ = area for heat exchange to cooling volume at ith station, in.^{2}
$A_{hx_{nozz,i}}$ = area of heat exchange to aerospike nozzle at ith station, in.^{2}
$a_{LH2,i}$ = liquid hydrogen Mach number at ith station
$a_{LOX,i}$ = liquid oxygen Mach number at ith station
F = thrust, lbf
g_0 = 32.18 ft/s^2
h_i = height of channel at ith station, in.
I_{sp} = specific impulse, s
l_c = chamber length, in.
l_i = length of station $= 0.2^* l_c$, in.
$\dot{m}$ = total mass flow, lbm/s
$\dot{m}_{LH2}$ = liquid hydrogen mass flow, lbm/s
$\dot{m}_{LOX}$ = liquid oxygen mass flow, lbm/s
m_{plug} = slope of aerospike plug
n = number of channels in cooling volume
p_i = fluid pressure at ith station, psia
r_{c_i} = inner radius of chamber, in.
$r_{ci,i}$ = inner radius of chamber at ith station, in.
$r_{c_o,i}$ = outer radius of chamber at ith station, in.
$r_{n,i}$ = radius of aerospike nozzle at ith station, in.
$r_{n,i-1}$ = radius of aerospike nozzle at, $i-1$th station, in.
r_{t_i} = inner radius at throat, in.
T_i = fluid temperature at ith station, R
$V_{cv,i}$ = volume of cooling volume at ith station, in.^{3}
w_i = half width of channel at ith station, in.
w_{init} = initial half width of channel, in.
x_i = normalized location of the ith station

Received 12 July 2010; revision received 1 November 2010; accepted for publication 1 November 2010.

*Ph.D. Student, Aero/Astro Engineering. Student Member.
†Assistant Professor, Aero/Astro Engineering. Associate Fellow.

I. Introduction

THE Air Force Institute of Technology (AFIT) is studying the dual-expander aerospike nozzle (DEAN) rocket engine architecture to significantly improve upper-stage rocket performance. The specific performance goals of this research are to provide 50,000 lbf vacuum thrust with a vacuum I_{sp} of 464 s. The DEAN, shown in Fig. 1, is a liquid hydrogen (LH2)/liquid oxygen (LOX) engine using separate expander cycles to pump the fuel and oxidizer and an aerospike nozzle to improve efficiency [1].

Previous work at AFIT by Martin focused on developing an initial design to demonstrate the feasibility of the DEAN architecture by building a computational model using the Numerical Propulsion System Simulation (NPSS^{TM}) software package [1]. That work culminated in a design exceeding the requirements. This paper outlines the current work at AFIT to optimize the DEAN's thrust-to-weight ratio (T/W) by expanding Martin's model through simplifying the calculations of the DEAN geometry and adding parametric variables to the model to support automated trade studies in ModelCenter^{TM}. The results of those trade studies indicate the DEAN can run at the specified performance using a lower total mass flow and a significantly shorter engine than the previous design.

II. Existing NPSS^{TM} DEAN Model

The original NPSS DEAN model was prepared by Martin as part of his masters thesis at AFIT [1]. This model uses NPSS elements to represent the pumps, turbines, pipes, valves, chamber, nozzle, and cooling channels to accurately model the DEAN architecture. The results of Martin's analysis converge to a working design, validating the DEAN concept. The DEAN thrust, I_{sp}, and T/W exceed both its requirements and the performance of the upper-stage single-expander cycle based RL10A-3 rocket engine, as can be seen in Table 1.

This excess in thrust performance suggests the dual-expander cycle offers an advantage in thrust over the single-expander cycle, and it indicates room to optimize the DEAN design further. Before discussing the changes made to Martin's model [1], necessary to facilitate this optimization, it is useful to review the key elements of the DEAN architecture and Martin's model.

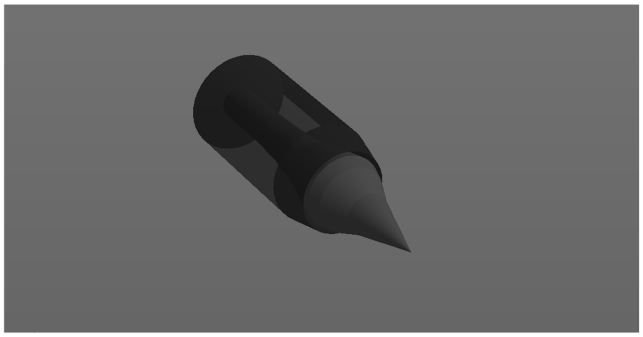

Fig. 1 Original DEAN geometry.

A. Existing DEAN Architecture

The DEAN uses two novel design choices. The first is the use of separate expander cycles for the fuel and the oxidizer. In a traditional expander cycle, the fuel is pumped through a cooling jacket for the chamber and nozzle. The heat picked up by the fuel from cooling the chamber and nozzle is then used to drive the turbine that runs both the fuel and oxidizer pumps, before the fuel is introduced into the chamber [3].

Figure 2 shows the DEAN's two separate expander cycles. The fuel loop is on the left. Here, the LH2 flows from the fuel tank into the first fuel pump. Half of the LH2 then flows through a bypass, while the remainder is fed into a second fuel pump. This flow then continues into the aerospike nozzle, where it absorbs heat while cooling the nozzle. The heated flow then drives the fuel turbine before joining with the bypass flow and entering the combustion chamber through the injector. On the right is the oxidizer loop. In this loop, the LOX flows from the oxidizer tank into the single oxidizer pump. This flow then enters the cooling jacket for the combustion chamber, where it absorbs heat while cooling the chamber. The heated oxygen then flows toward the oxidizer turbine, with a small amount (roughly 10%) sent around the turbine using a bypass and the remainder used to drive the turbine. Finally, the oxygen flows are joined before entering the combustion chamber through an injector [1].

The two separate expander cycles present benefits and challenges. Increased chamber pressures and, in turn, engine performance can be obtained by separating the power demands between two separate turbines driven by separate working fluids. The separate expander cycles also ensure the fuel and oxidizer remain physically separated until entering the combustion chamber, eliminating one of the more catastrophic failure modes in traditional expander cycles, namely, failure of an interpropellant seal [1]. However, the LOX cycle requires a turbine material that will work well in an oxygen environment. Additional research at AFIT showed that Inconel 718 provides both satisfactory oxygen resistance and suitable mechanical performance for use in both the pump and the turbine in the LOX cycle [4].

The second novel design choice is the use of an aerospike, or plug, nozzle. Traditional bell nozzles are optimized to perform at a single pressure or altitude. This optimization makes them very efficient at their design point but much less so for the remainder of the flight. Aerospike nozzles on the other hand, due to their geometry, adapt their performance to the current altitude. Even though aerospike nozzles perform less efficiently than bell nozzles at the design altitude of a given bell nozzle, when considering the altitudes seen by a launch vehicle, the global performance of an aerospike nozzle exceeds the global performance of a bell nozzle, making the aerospike nozzle an attractive design for launch vehicles. More important, for the DEAN, the use of an aerospike nozzle provides a second, physically separate cooling loop from the chamber for use in the second expander cycle. This second cooling loop increases the surface area inside the chamber used to drive the turbomachinery, providing for correspondingly increased power to the pumps and increased chamber pressure and, in turn, increased engine performance [1]. The aerospike nozzle is also shorter and lighter than a traditional bell nozzle, leading to improved packaging and T/W. Finally, the DEAN architecture is a forerunner to similar boost stage architecture, where the aerospike nozzle's global performance will result in even greater gains than in an upper-stage engine.

B. NPSS^{TM} Model Details

NPSS is a computer simulation tool for modeling aircraft and rocket engines. Engine simulations built in NPSS provide higher fidelity results than engine cycle studies. NPSS has been developed by the NASA Glenn Research Center, with assistance from the aerospace propulsion industry. Models built in NPSS consist of a series of interconnected software objects representing the components of the engine under consideration. The object connections are made using NPSS application programming interfaces modeling fluid flows, mechanical connections, and thermal flows called ports. A built-in solver in NPSS can then be used to drive the model design variables to balance the fluid flows, mechanical connections, and thermal flows in the model and converge on a design point [5].

Martin's model [1] of the DEAN engine includes elements to simulate the various components of the engine. The combustion chamber is modeled using a RocketComb1 element, which requires the chamber radius and volume. The RocketComb element also includes ThermalOutputPorts to model heat exchange to the fuel and oxidizer. The ThermalOutputPorts require the radius at the port's location, the cross-sectional area of the combusting flow in the chamber, and the surface area of the portion of the chamber in contact with the combusting flow. The model calculates the heat exchange between the chamber walls for the oxidizer expander cycle and the internal portion of the aerospike for the fuel expander cycle. The aerospike nozzle is modeled using a RocketNozzle element, which requires the throat area and the expansion ratio and includes more ThermalOutputPorts for use in the heat exchange between the aerospike and the fuel expander cycle.

The fuel and oxidizer tanks are modeled using Starter elements. The plumbing connecting the engine components to the tanks and each other is modeled using Valve04 elements that require the cross-sectional area to model the pressure drop in the plumbing and customized CoolingVolume elements, which require the cross-sectional area and fluid volume to model the heat loss in the lines. The cooling jackets around the combustion chamber and the aerospike nozzle are modeled using the ThermalOutputPorts in the chamber and nozzle and the plumbing elements connected by Wall2 elements. The pumps are modeled using customized Pump elements, which require the efficiency, pressure ratio, and mass flow of each pump. Finally, the turbines are modeled using customized Turbine elements, which require the efficiency, pressure ratio, mass flow, and the cross-sectional area of the flow.

While the cooling jackets in the DEAN are continuous volumes, the NPSS model represents them as a series of eight discrete stations. Figure 3 shows the locations of these stations in the model. The chamber (24 in. long in Martin's design [1]) consists of five equally spaced sections, with stations (represented by stars) at the midpoint of each section plus a station at the throat of the rocket. Note that the oxidizer loop (the outer wall of the chamber) and the fuel loop (the aerospike) are represented by separate sets of stations. The external portion of the aerospike (14 in. long in Martin's design) has two

Table 1 Existing DEAN design results versus requirements

	DEAN [1]	Requirement [1]	Percent difference, %	RL10A-3-3A [2]	Percent difference, %
Vacuum thrust	57,231 lbf	50,000 lbf	+14.5	16,500 lbf	+247
Vacuum I_{sp}	472 s	464 s	+1.7	443 s	+6.5
T/W	119	106	+12	53	+124

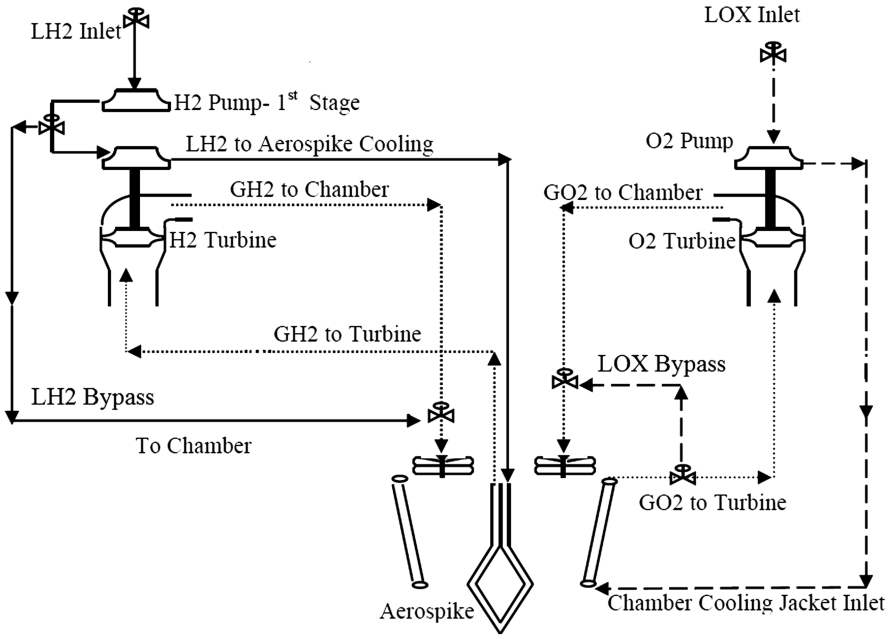

Fig. 2 DEAN architecture.

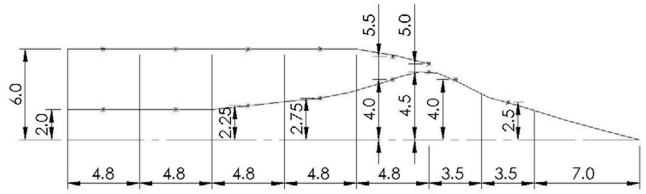

Fig. 3 DEAN geometry (dimensions in inches) (credit Martin [1]).

additional stations in the first half of the nozzle that are only in the fuel loop.

NPSS models have four classes of variables: the dependent variables the NPSS solver will ensure equal specified values, the independent variables the NPSS solver is free to adjust as necessary to converge the design, component inputs read by the NPSS solver but not altered by it, and component outputs calculated by the NPSS solver but not driven toward a particular value. Taken together, the NPSS dependent variables and component inputs form the set of user-specified design choices or design variables. The NPSS independent variables and component outputs form the set of user-specified responses or response variables. In the previous model, the design variables included the user-specified dependent variables (the pressure ratios for the three pumps) and the component inputs (for example, the volume of the combustion chamber and the nozzle expansion ratio). The response variables include the user-specified independent variables (the efficiencies of the first LH2 pump and of the LOX pump) and the component outputs (for example, the vacuum thrust and I_{sp}). Table 2 summarizes the design and response variables of the previous model.

Follow-on research at AFIT focusing on designs for the LH2 and LOX pumps provides verification for the NPSS model of the DEAN. In each design study, the respective expander cycle is modeled using spreadsheet calculations and Pumpal®/RITAL®. These additional models agree well with the NPSS model. For example, the Pumpal model of the LH2 pumps shows the required power of the first pump

Table 2 Existing DEAN design point [1]

Design variables		Response variables	
LOX pump pressure ratio, $PR_{p,LOX}$	103	Vacuum thrust (F_{vac}	57,000 lbf
LH2 pump 1 pressure ratio, $PR_{p,LH2,1}$	45	Vacuum I_{sp}	472 s
LH2 pump 2 pressure ratio, $PR_{p,LH2,2}$	2	Total mass flow, $\dot{m}$	121 lbm/s
LH2 pump 2 efficiency, $\eta_{p,LH2,2}$	0.83	O/F	7.03
Chamber length, l_c	24 in.	Chamber pressure, P_0	1739 psia
Outer chamber radius, r_{c_o}	6 in.	Chamber temperature, T_0	6586 R
Inner chamber radius, r_{c_i}	2 in.	LOX pump efficiency, $\eta_{p,LOX}$	0.66
Chamber volume, V_c	2075 in.^{3}	LOX pump power	2587 HP
Throat area, A_t	15.9 in.^{2}	LH2 pump 1 efficiency, $\eta_{p,LH2,1}$	0.67
Nozzle length, l_n	14 in.	LH2 pump 1 power	2527 HP
Expansion ratio, ϵ	125	LH2 pump 2 power	1046 HP
		LOX turbine pressure ratio, $PR_{t,LOX}$	1.82
		LOX Turbine efficiency, $\eta_{t,LOX}$	0.949
		LOX turbine power	2587 HP
		LH2 turbine pressure ratio, $PR_{t,LH2}$	1.84
		LH2 turbine efficiency, $\eta_{t,LH2}$	0.9
		LH2 turbine power	3573 HP
		LOX temperatures, $T_{LOX,i}$	179–617 R
		LOX pressures, $P_{LOX,i}$	3810–4500 psia
		LOX max Mach number, $M_{max,LOX}$	0.56
		LH2 temperatures, $T_{LH2,i}$	145–610 R
		LH2 pressures, $P_{LH2,i}$	3670–4000 psia
		LH2 max Mach number, $M_{max,LH2}$	0.67

is 2523 HP (less than 1% difference from the NPSS value), and the required power of the second pump is 1079 HP (approximately 3% difference from the NPSS model). Furthermore, the pressure coming out of the second pump is 4050 psia versus 4000 psia in the NPSS model (approximately 1% difference) [6]. The LOX pump values show similar agreement. For example, the Pumpal model of the LOX pump shows the required power is 2215 HP (approximately 12% difference from the NPSS model), and the pressure coming out of the LOX pump is 4600 psia versus 4500 psia in the NPSS model (approximately 2% difference) [4].

Given the importance of balancing the heat and mechanical flows in an expander cycle, it is worth noting the performance of the turbomachinery in existing DEAN design. Naturally, the converged design point balances the power required by the pumps with that provided by the turbines for each of the two expander cycles. While the performance of the turbomachinery may appear high when compared with RL10A, which provides only 789 HP from its turbine, Pratt and Whitney built an LH2 expander cycle that produces 5900 HP as part of an upper-stage demonstrator engine [6]. This puts the LH2 cycle well within demonstrated capability. As for the LOX cycle, research at AFIT has proposed designs for the LOX pump and turbine that provide the required performance as a part of this architecture [4].

III. Parametric NPSS^{TM} DEAN Model

The goal of the current research at AFIT is to optimize the DEAN engine to provide the maximum T/W, while maintaining the required thrust and I_{sp}, and not violating operational limits for the materials and working fluids. The T/W can be maximized by either increasing the thrust or decreasing the weight. Since the DEAN has a fixed thrust requirement, the optimization problem can be restated as optimizing the DEAN engine to provide the minimum weight, subject to the previously mentioned constraints. Identifying the design variables driving the weight of the engine and updating the model to use those variables as the design variables enables automated searching over the design trade space for optimal designs.

The rocket engine chamber, nozzle, and turbomachinery are the elements used to estimate the total mass (weight) of the rocket engine during conceptual design. The chamber and nozzle masses are driven by their geometry and material, while the turbomachinery masses are driven by their local mass flows [3]. The model previously captured the geometry of the DEAN as hard-coded values, tying the model to a single design point. Additionally, the model treated the mass flows as

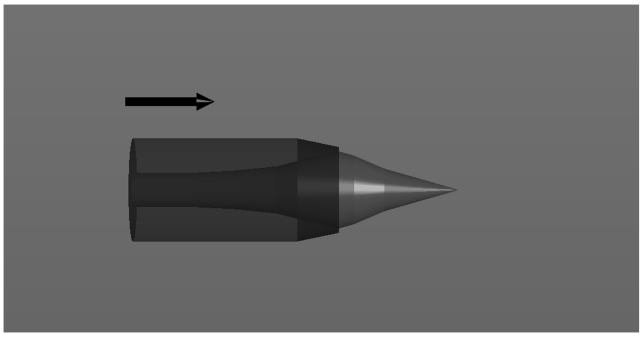

a) Martin's [1] geometry for the DEAN

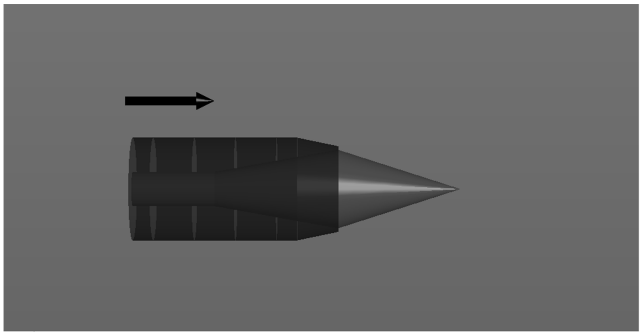

b) Parametric geometry with simplified aerospike

Fig. 5 Comparison of simplified geometry to Martin's [1] original geometry.

responses. To use the model to optimize the design, the NPSS model must be altered to use the chamber and nozzle geometries and the local mass flows to the turbomachinery as design variables. This section details the modifications made to the previous model to convert it into a parametric model based on the design variable needs and two changes made while the NPSS model was being modified to reflect the most recent DEAN architecture being considered.

A. Updated DEAN Architecture

Before modifying the DEAN model to support parametric trade studies, two architecture changes were made to the fuel expander

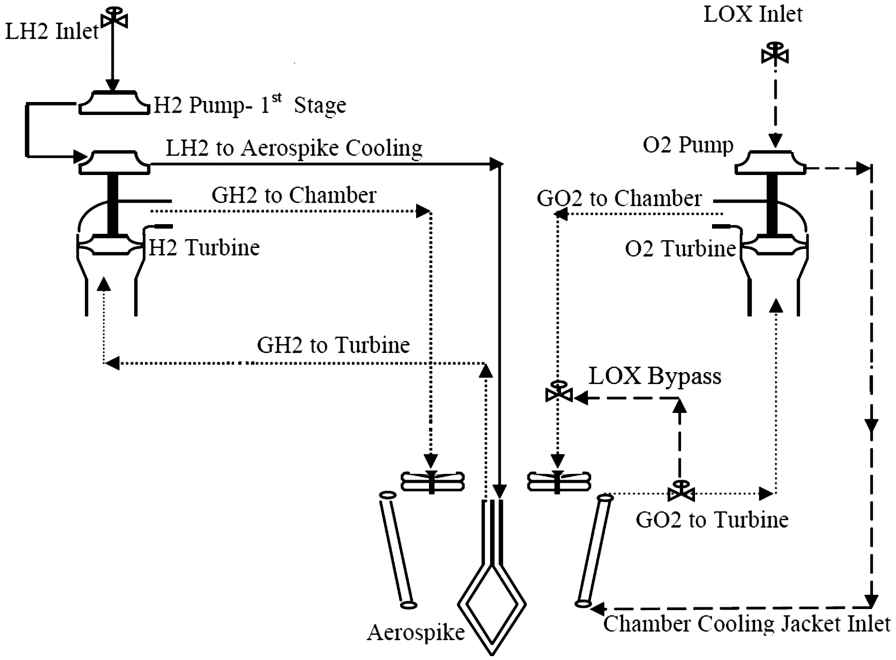

Fig. 4 Updated DEAN architecture.

Table 3 Parametric study over LH2 pump 1 pressure ratio

Design variables		Response variables	
LOX pump pressure ratio, $PR_{p,LOX}$	103	Vacuum thrust, F_{vac}	49,500–60,000 lbf
LH2 pump 1 pressure ratio, $PR_{p,LH2,1}$	30–60	Vacuum I_{sp}	416–491 s
LH2 pump 2 pressure ratio, $PR_{p,LH2,2}$	2	Total mass flow, $\dot{m}$	119–132 lbm/s
LH2 pump 2 efficiency, $\eta_{p,LH2,2}$	0.83	O/F	4.2–11.3
Expansion ratio, ϵ	125	Chamber pressure, P_0	1500–1940 psia
		Chamber temperature, T_0	5000–6660 R

cycle to reflect refinements in the design. Figure 4 shows this updated DEAN architecture. The first change was to remove the LH2 bypass, feeding the cooling jacket for the aerospike with the full mass flow of the LH2 instead of only half. The second change was to require the two fuel pumps to run at the same pressure ratio to minimize the maximum pressure ratio required for the fuel pumps.

B. NPSS™ Model Details

The modifications to convert the NPSS DEAN model into a parametric model involved the chamber and nozzle geometry and the mass flows through the turbomachinery. The system-level parameters chosen to drive the chamber and nozzle geometries are the chamber length, the inner and outer chamber radii, and the shape of the nozzle. A number of intermediate geometric values are determined by the shape of the nozzle. To facilitate calculating these values, the geometry of the aerospike and cooling volumes were simplified to linear approximations from their higher-order calculations (the aerospike radii are calculated using the method of characteristics [1]). Figure 5 compares the results of these simplifications to the original geometry.

The calculations based on these simplifications include the radius of the aerospike at each station [Eq. (2)], the combusted flow cross-sectional area [Eq. (3)], the surface area of the heat exchanges for the chamber [Eq. (4)], the aerospike nozzle [Eq. (5)] and cooling volumes [Eq. (9)], the cross-sectional area [Eq. (10)], and the volume of the fluid in the cooling volumes [Eq. (11)]. These values are calculated from the inner and outer radii of the chamber and the throat, the chamber and aerospike lengths, the cooling channel half widths and half spacings, and the aspect ratios (ARs):

$$m_{\text{plug}} = (r_{t_i} - r_{c_i})/(0.6 * l_c) \tag{1}$$

$$r_{c_i,i} = r_{c_i} + m_{\text{plug}} \cdot x_i \cdot l_c \tag{2}$$

$$A_{\text{flow},i} = \pi \cdot (r_{c_o,i}^2 - r_{c_i,i}^2) \tag{3}$$

$$A_{\text{hx}} = 2 \cdot \pi \cdot r_{c_o,i} \cdot l_i \tag{4}$$

$$A_{\text{hx}_{\text{nozz}},i} = \pi \cdot (r_{n,i} + r_{n,i-1}) \cdot \sqrt{(r_{n,i} + r_{n,i-1})^2 + l_i^2} \tag{5}$$

$$n = \text{round}[\pi \cdot r/(w_{\text{init}} + a)] \tag{6}$$

$$w_i = \pi \cdot r/n_{\text{channels}} + a \tag{7}$$

$$h_i = 2 \cdot w_i \cdot \text{AR} \tag{8}$$

$$A_{\text{hx}_{\text{cv},i}} = 2 \cdot w_i \cdot n \cdot l_i \tag{9}$$

$$A_{\text{cv},i} = 2 \cdot w_i \cdot h_i \cdot n \tag{10}$$

$$V_{\text{cv},i} = A_{\text{cv},i} \cdot l_i \tag{11}$$

The system-level parameters chosen to drive the mass flows to the turbomachinery are the O/F ratio and total mass flow. These parameters also drive the performance constraints of thrust and I_{sp}. Equation (12) [3] determines the LOX mass flow from these system-level parameters, and Eq. (13) [3] determines the LH2 mass flow. In the original model, the O/F ratio can only be controlled indirectly by changing the pressure ratios of the pumps, leading to coupling effects appearing in the O/F plots. For example, a parametric study, described in Table 3, varied the pressure ratio of the first LH2 pump:

$$\dot{m}_{\text{LOX}} = \frac{\text{O/F}}{1 + \text{O/F}} \cdot \dot{m} \tag{12}$$

$$\dot{m}_{\text{LH2}} = \frac{1}{1 + \text{O/F}} \cdot \dot{m} \tag{13}$$

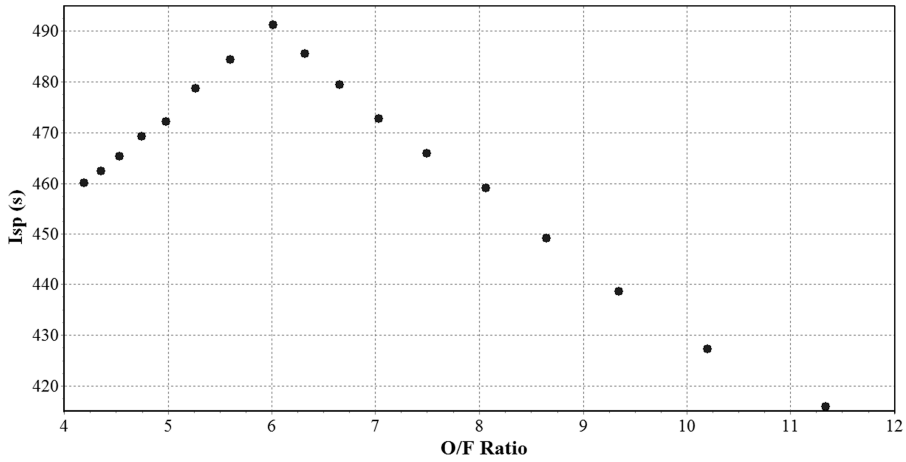

Fig. 6 I_{sp} vs O/F, original NPSS model.

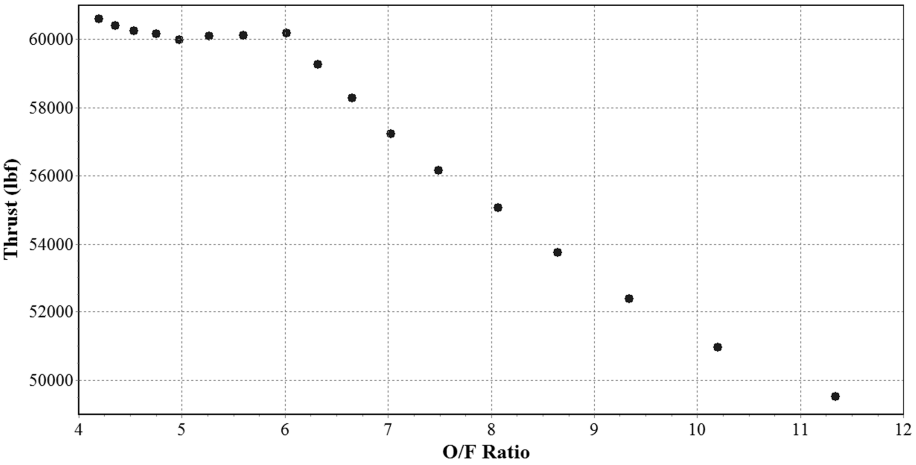

Fig. 7 Thrust vs O/F, original NPSS model.

Figure 6 shows the relationship between I_{sp} and O/F for the DEAN based on this parametric study. The peak I_{sp} is at an O/F ratio of approximately six. Ordinarily, this result would be produced by a parametric study as a function of the independent variable, O/F, implying the total mass flow was constant. Equation (14) [3] supports the conclusion that thrust versus O/F would follow the trend in Fig. 6. However, Fig. 7 shows a peak at an O/F of six and then a rise toward another peak for $O/F < 5$:

$$I_{sp} = \frac{F}{\dot{m} g_0} \tag{14}$$

The deviation from the describing equations rests with the assumption of constant total mass flow. Figure 8 is a three-dimensional plot showing thrust versus both O/F and total mass flow. The vertical axis is the thrust, the left axis is O/F, and the back axis is the total mass flow. The starred point is O/F equals six. The total mass flow has a sharp turn as O/F decreases beyond that point, leading to the second increase in thrust as total mass flow reaches its peak during the parametric study. To eliminate coupling effects like this example, and an instability in the LH2 efficiencies, the user-defined dependent variables were changed to the total mass flow and an equation setting the two fuel pumps to the same pressure ratio. The user-defined independent variables were changed to the throat area and to the pressure ratios for all three pumps.

One final change was made to the NPSS model. In the model, the mass flow through the oxidizer bypass was hard coded to a specific value, resulting in instabilities in the model when the system mass flow or the O/F ratio changed. The oxidizer mass flow through the bypass was set to be 10% of the oxidizer mass flow, and the mass flow to the oxidizer turbine was set to 90%. These percentages were also made user configurable.

IV. System-Level DEAN Model

A system-level model of the DEAN engine was built around the parametric NPSS model in order to run automated trade studies. This system-level DEAN model was built in ModelCenter™. ModelCenter is a multidisciplinary modeling environment used to study the trade space of a design and optimize that design. ModelCenter can combine analyses developed in a variety of tools, including MATLAB, Mathcad, Excel, and command line executables (for

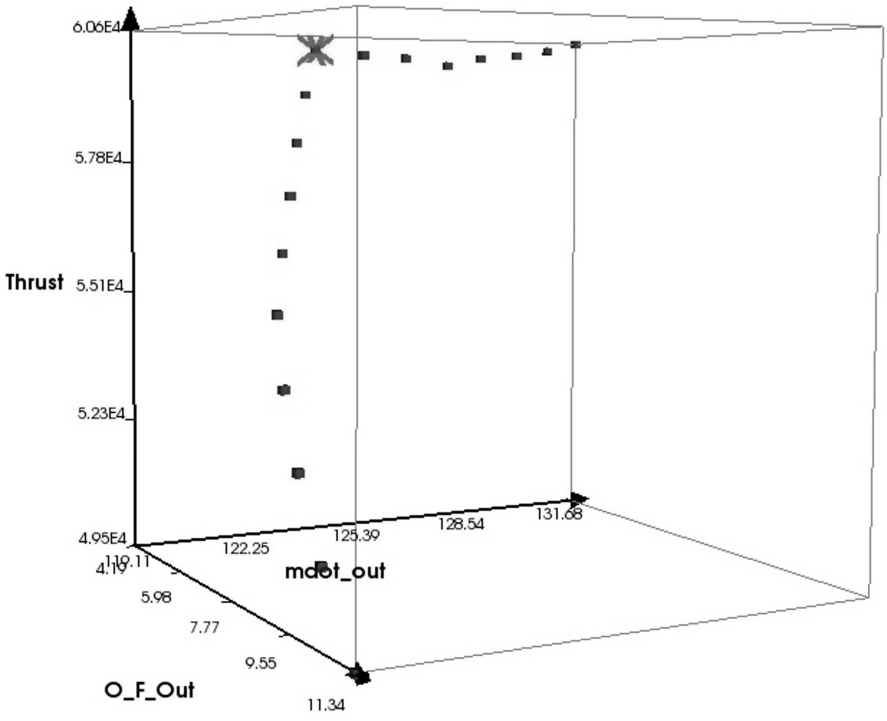

Fig. 8 Thrust vs O/F and total mass flow, original NPSS model.

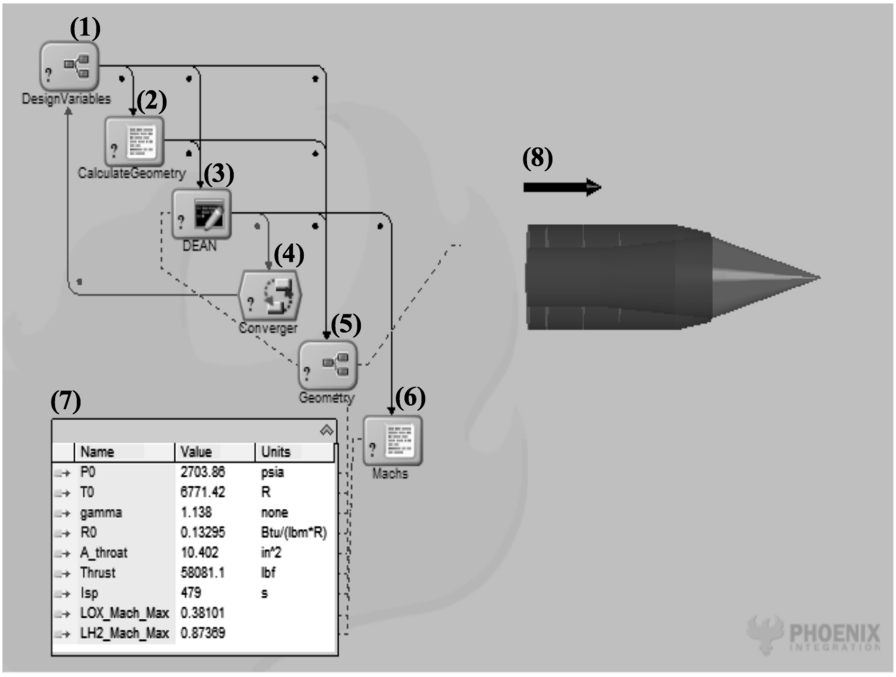

Fig. 9 System-level model of DEAN.

example) into a single system-level model. Users can then use the built-in trade study and visualization tools to conduct sensitivity studies to gain insight into what aspects of the design are the key drivers influencing the desired results. ModelCenter also provides a rich set of built-in optimization tools used to find values for the key drivers optimizing the design for a given goal (such as minimizing the mass of the DEAN engine) while ensuring constraints are not violated (such as maintaining the required thrust and I_{sp}). These optimization tools include a gradient optimizer, a genetic optimizer called Darwin™, and an optimizer that uses surrogate models of the design space during optimization called DesignExplorer™ [7].

Figure 9 shows the system-level DEAN model in the ModelCenter interface. The model consists of six components and two data display elements. Table 4 summarizes these components.

The first four components in the DEAN system-level model are used to run the DEAN NPSS model. The first component stores the system-level design variables. They are the total mass flow, the O/F ratio, the inner chamber radius, the outer chamber radius, the chamber length, and a guessed value for the throat area. The second component calculates the nozzle radius using Eq. (3), a nozzle length based on the slope of the aerospike nozzle, and the chamber volume using volume equations for cylinders and cones from the design variables. The third component runs the NPSS DEAN model using the values of the design variables and the values calculated in the CalculateGeometry component. Since the throat area is an independent variable in the NPSS model, the NPSS solver may select a value that does not match the guessed value. If the model chooses such a value, the geometry values calculated from the guessed throat area (specifically, the nozzle radius and cooling volume sizes) are incorrect. The fourth component addresses this problem using a direct substitution iteration solver. The solver directs the system-level model to be run in a loop, substituting the NPSS calculated throat area for the guessed throat area until the two are the same value, closing the design.

Table 4 System-Level DEAN Model Components

Label	Name	Description
1	Design variables	A component storing the system-level design variables
2	Calculate geometry	A script component calculating the geometry parameters for the DEAN model from the design variables
3	DEAN	The parametric NPSS DEAN model imported into the ModelCenter framework using the embedded Quick Wrap tool
4	Converger	A direct substitution convergence loop used to converge the guessed throat area to the calculated throat area
5	Geometry	A collection of geometry primitives (surfaces of revolution and an arrow) and a script component to render the live view of the DEAN geometry seen in Eq. (8)
6	Mach numbers	A script component that uses polynomial interpolation to calculate the Mach numbers for the LOX and LH2 fluid flows in the cooling volumes
7	Data monitor	A built-in ModelCenter component set to display the key performance values from the DEAN model
8	Geometry rendering	A live preview of the DEAN geometry based on the geometry components in Eq. (5)

The remaining two components in the DEAN system-level model are used for postprocessing the DEAN NPSS model. The fifth component is actually four components that are part of a ModelCenter assembly component. ModelCenter assembly components allow model developers to group related components together to simplify the display and management of the model. Three of the four subcomponents in the geometry component are built-in ModelCenter geometry primitives: two surfaces of revolution to render the chamber, the aerospike, and a 12-in.-long arrow to provide a scale for the DEAN geometry. The final subcomponent is a ModelCenter script component transforming the output from the DEAN NPSS model into geometry strings that define the curves for the surface of revolution components.

The last analysis component calculates the Mach numbers for the LOX and LH2 fluid flows in the cooling volumes. These values are critical constraints on the engine design, as the flows cannot be allowed to reach sonic conditions. Previous constraints for these values were a maximum Mach number in the LOX flows of 0.6 and a maximum Mach number in the LH2 flows of 0.9 [1]. Martin [1] calculated the Mach numbers at each station by looking up the speed of sound for the fluids in the Thermophysical Properties of Fluid Systems online handbook[‡], from the National Institute of

[‡]Available at http://webbook.nist.gov/chemistry/fluid/ [retrieved 27 May 2010].

Table 5 DOEs over O/F, total mass flow, and chamber length

Design variables		Response variables	
O/F	5.5–7.5	Vacuum thrust, F_{vac}	39,700–69,500 lbf
Total mass flow, $\dot{m}$	85–140 lbm/s	Vacuum I_{sp}	466–499 s
Chamber length, l_c	22–30 in.	Chamber pressure, P_0	1798–3243 psia
Outer chamber radius, r_{c_o}	6 in.	Chamber temperature, T_0	6130–6850 R
Inner chamber radius, r_{c_i}	2 in.	Throat area, A_t	7.2–17.5 in.^{2}
Expansion ratio, ϵ	125	Nozzle length, l_n	13.7–14.8 in.
LOX bypass, %	90	Chamber volume, V_c	1810–2480 in.^{3}
LOX pump efficiency, $\eta_{p,\mathrm{LOX}}$	0.773	LOX temperatures, T_{LOX}	162–886 R
LOX turbine efficiency, $\eta_{t,\mathrm{LOX}}$	0.949	LOX pressures, p_{LOX}	2865–5864 psia
LH2 pump 1 efficiency, $\eta_{p,\mathrm{LH2},1}$	0.8	LH2 temperatures, T_{LH2}	73–634 R
LH2 pump 2 efficiency, $\eta_{p,\mathrm{LH2},2}$	0.83	LH2 pressures, p_{LH2}	3220–10,750 psia
LH2 pump efficiency, $\eta_{p,\mathrm{LH2}}$	0.9		

Table 6 Data ranges for speed-of-sound tables

Fluid	Temperatures, R	Pressure range, psia, step size = 100 psia
LOX	150, 275, 400, 525 650, 775, 900	2800–6000
LH2	70, 165, 260, 355 450, 545, 640	3200–7200

Standards and Technology, based on the fluid temperatures and pressures. The Mach number component automates this process by using third-order polynomials to interpolate the speed of sound for LOX and LH2 over the temperature and pressure ranges seen in the DEAN model. Table 5 summarizes the design of experiments (DOEs) trade study used to establish these ranges.

To create the interpolation polynomials, a set of isothermal speed-of-sound versus pressure tables for both oxygen and hydrogen were downloaded from the Thermophysical Properties of Fluid Systems online handbook. Table 6 shows the temperatures and pressures selected for these tables. Note, the LH2 pressure range was truncated after determining pressures above 7200 psia represented designs no longer being considered.

The speed-of-sound tables were then imported into ModelCenter for surface fitting using the data import plug in. The interpolation polynomials were then created by running a cubic fit to the data in ModelCenter's response surface modeling (RSM) toolkit. Equation (15) shows the polynomial generated for the speed of sound in LOX, and Eq. (16) shows the polynomial generated for the speed of sound in LH2. Both equations are good fits to the data, as can be seen from their adjusted R^2 values and a graphical comparison with the results from the earlier design. Equation (15) has an adjusted R^2 value of 0.995, and Eq. (16) has an adjusted R^2 value of 0.988. Figure 10 shows that Mach numbers calculated from both equations also compare favorably to results from the earlier design of the DEAN:

$$a_{\mathrm{LOX},i} = 6009.519 - 25.08448T_i + 0.05203138p_i + 0.03725712T_i^2 + 0.0004540472T_ip_i - 1.669077 \cdot 10^{-05}T_i^3 - 5.292126 \cdot 10^{-07}p_iT_i^2 \tag{15}$$

$$a_{\mathrm{LH2},i} = 4014.306 - 15.03106T_i + 0.7100687p_i + 0.04704292T_i^2 - 2.660187 \cdot 10^{-05}p_i^2 - 0.0009330969T_ip_i - 3.34523 \cdot 10^{-05}T_i^3 + 4.862856 \cdot 10^{-08}T_ip_i^2 \tag{16}$$

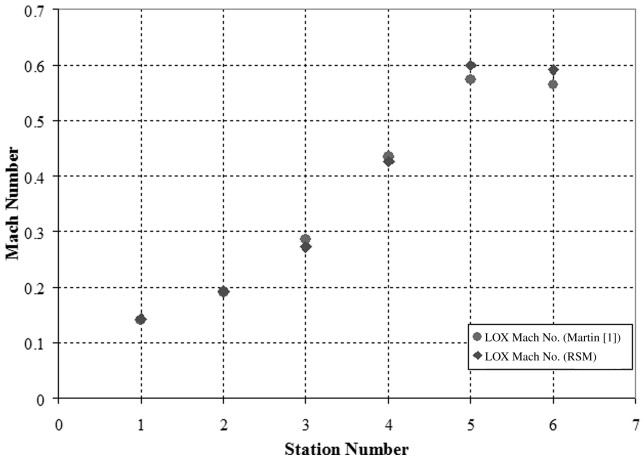

a) LOX mach numbers

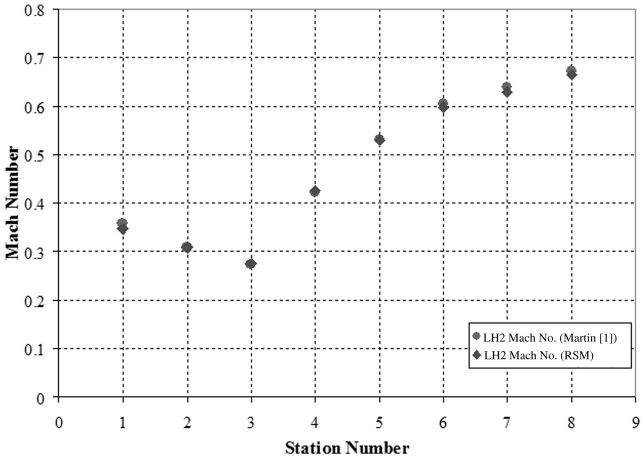

b) LH2 mach numbers

Fig. 10 Comparison of fluid Mach number calculations.

V. Results and Analysis

The analysis of the system-level DEAN model took place in two phases. First, parametric studies were run over the chamber length, the O/F ratio, and the total mass flow to establish the boundaries of the design trade space. The results of the parametric studies were then used to scale the original DEAN design to more closely match the performance goals.

A. Parametric Studies

Table 7 summarizes the first parametric study of the DEAN system-level model, which varied the O/F ratio from 5.5 to 7.5. Initial results from this trade study are promising. The plot of I_{sp} versus O/F in Fig. 11 shows the peak I_{sp} occurs at an O/F ratio of approximately six, just as in the previous study shown in Fig. 6.

However, the maximum LH2 Mach numbers exceed the constraint value established by Martin [1] across the entire parametric study, as can be seen in Fig. 12. A review of the LH2 Mach numbers at all of

Table 7 Parametric over O/F

Design variables		Response variables	
O/F	5.5–7.5	Vacuum thrust, F_{vac}	56,700–60,000 lbf
Total mass flow, $\dot{m}$	121.25 lbm/s	Vacuum I_{sp}	468–495 s
Chamber length, l_c	24 in.	Chamber pressure, P_0	2135–2415 psia
Outer chamber radius, r_{c_o}	6 in.	Chamber temperature, T_0	6180–6705 R
Inner chamber radius, r_{c_i}	2 in.	Throat area, A_t	12.1–12.8 in.^{2}
Expansion Ratio, ϵ	125	Nozzle length, l_n	14.2–14.3 in.
LOX bypass, %	90	Chamber volume, V_c	1576–1579 in.^{3}
LOX pump efficiency, $\eta_{p,\mathrm{LOX}}$	0.773	LOX temperatures, T_{LOX}	166–657 R
LOX turbine efficiency, $\eta_{t,\mathrm{LOX}}$	0.949	LOX pressures, p_{LOX}	3860–4380 psia
LH2 pump 1 efficiency, $\eta_{p,\mathrm{LH2},1}$	0.8	Max LOX Mach number	0.40–0.41
LH2 pump 2 efficiency, $\eta_{p,\mathrm{LH2},2}$	0.83	LH2 temperatures, T_{LH2}	85–436 R
LH2 pump efficiency, $\eta_{p,\mathrm{LH2}}$	0.9	LH2 pressures, p_{LH2}	4590–8340 psia
		Max LH2 Mach number	0.99–1.20

the stations reveals the Mach numbers are within acceptable limits for nozzle radii greater than 3.3 in. To test this conclusion, the inner chamber radius was increased from 2.0 to 3.3 in. However, the NPSS model could not converge, because some of the LH2 cooling volumes had become too large. Addressing this result, several cooling volume AR calculations were adjusted until the model converged. As expected, the maximum LH2 Mach number for this new design fell within the constraint value of 0.9. Running the parametric study with the adjusted ARs resulted in maximum LH2 Mach numbers between 0.81 and 0.88, enabling continued exploration of the DEAN trade space.

Figure 13 is the plot of I_{sp} versus O/F ratio for the updated inner chamber radius. The added detail in this plot shows the O/F ratio for maximum I_{sp} is between 5.9 and 6.1, higher than might be expected (just based on the O/F ratio), given the RL10 upper-stage engine runs at an O/F ratio of 5.0 [3]. However, while the total mass flow and most of the geometric parameters are constant in Fig. 13, the chamber pressure and temperature are not. Figure 14 shows how chamber pressure varies with O/F, and Fig. 15 shows how the chamber temperature varies with O/F. The chamber pressures seen in Fig. 14 range from 2625 to 2875 psia. These values are considerably higher than the 640 psia of the RL10B-2 [3], or even the practical limits of a

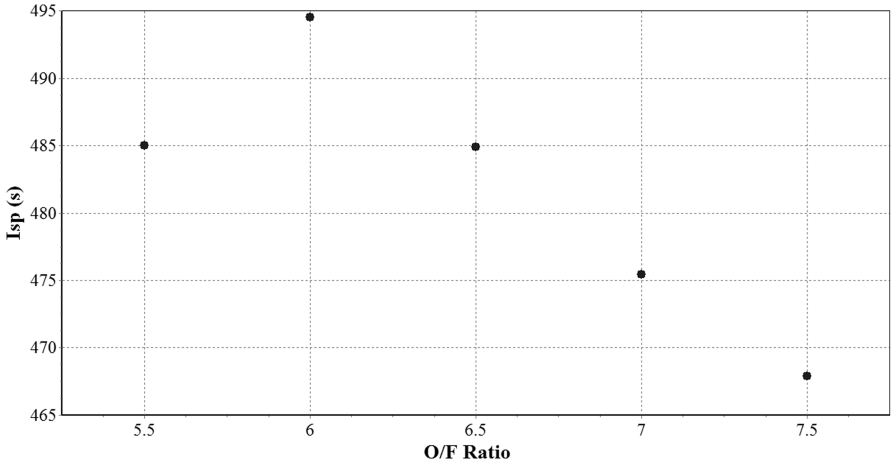

Fig. 11 I_{sp} vs O/F ratio, system-level model.

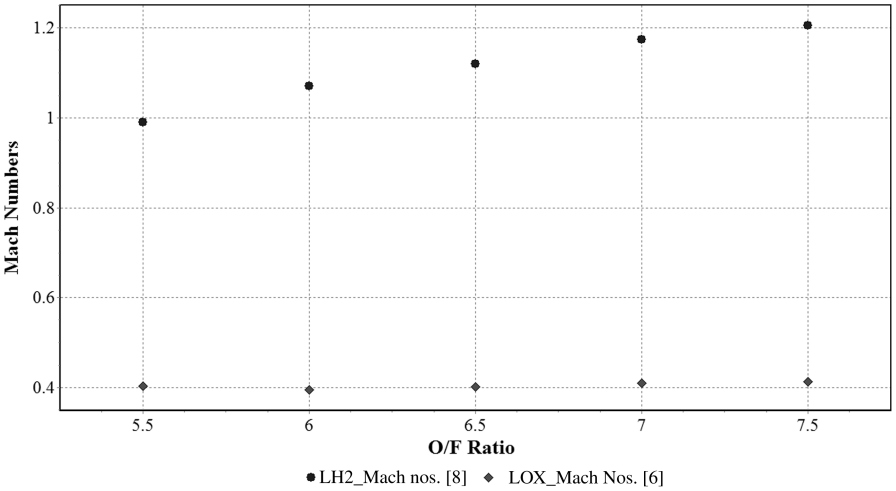

Fig. 12 Fluid mach numbers vs O/F ratio, system-level model.

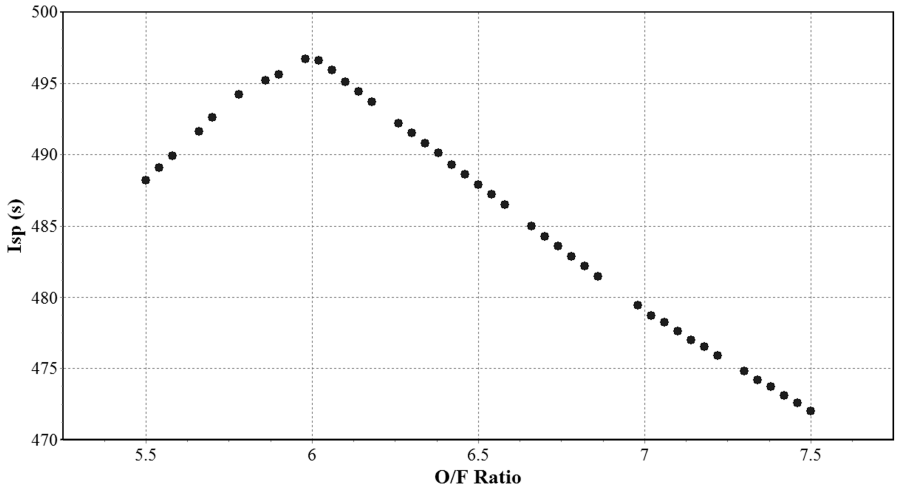

Fig. 13 Detailed I_{sp} vs O/F ratio, system-level model.

single-expander cycle LOX/LH2 engine, which Krach and Sutton determined to be between 1375 and 2300 psia [8]. This dramatic difference in chamber pressures suggests higher chamber pressures are possible with the dual-expander cycle of the DEAN architecture than with single-expander cycles.

Figure 16 uses a three-dimensional plot with varying shades of gray on the data points to present all four of these variables, I_{sp}, O/F, chamber pressure, and chamber temperature, in a combined plot to present a unified view of their interactions. The O/F ratio is on the left axis, the chamber pressure is on the rear axis, and I_{sp} is on the vertical axis. Finally, the chamber temperature is shown as the shades of the data points. This figure shows the maximum I_{sp} not only happens at an O/F of six but also at the maximum chamber pressure and somewhere in the middle of the chamber temperature range seen

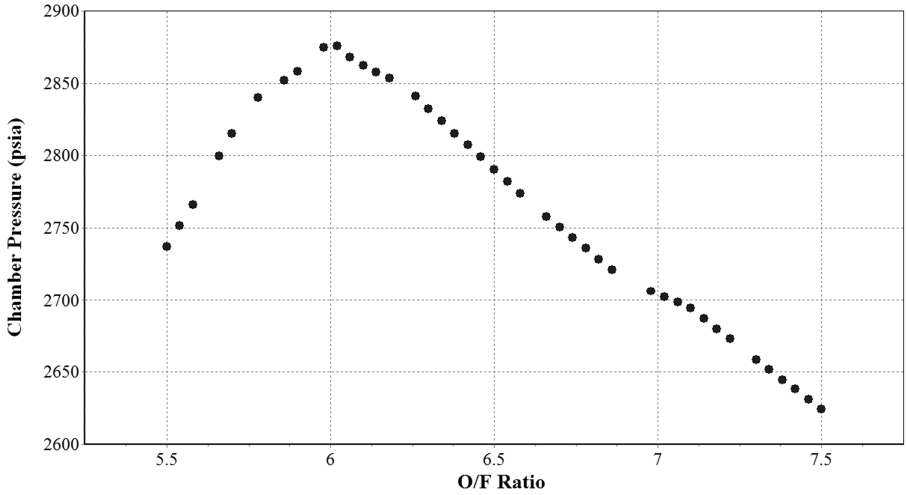

Fig. 14 Detailed chamber pressure vs O/F ratio, system-level model.

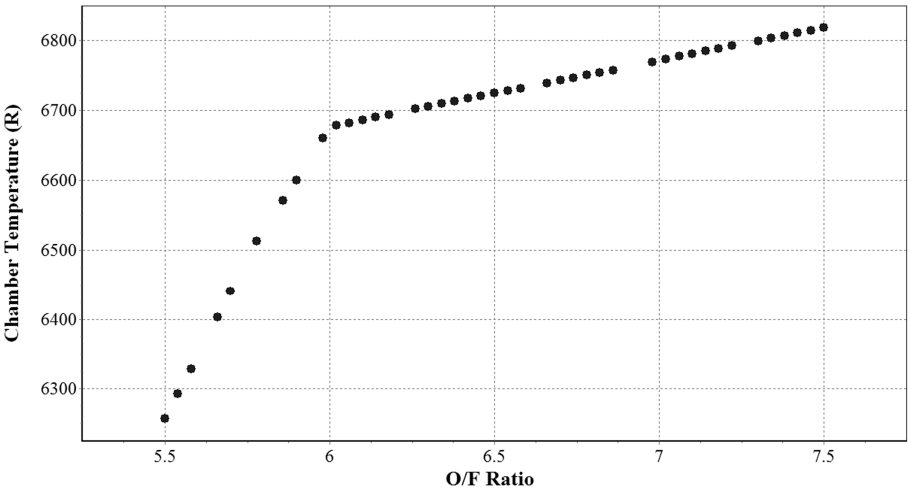

Fig. 15 Detailed chamber temperature vs O/F ratio, system-level model.

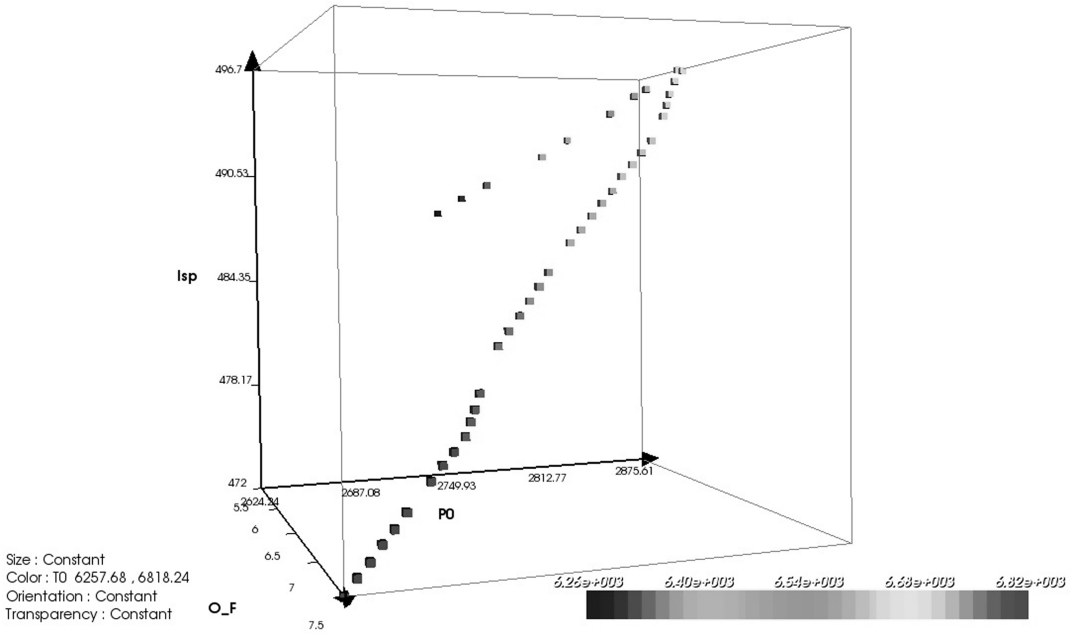

Fig. 16 I_{sp} vs O/F ratio, chamber pressure, and chamber temperature, system-level model.

in this study. Returning to Fig. 15 reveals the chamber temperature for the O/F where the maximum I_{sp} occurs is located at a knee in the temperature curve. The trends evident in Fig. 16 suggest the solution is simply one possible curve on a solution surface space.

Table 8 summarizes the second parametric study run of the DEAN system-level model, which varied the total mass flow from 85 to 122 lbm/s. As one would expect, thrust is linearly related to total mass flow (Fig. 17). A total mass flow of only 104 lbm/s is sufficient

Table 8 Parametric over total mass flow

Design variables		Response variables	
O/F	7	Vacuum thrust, F_{vac}	40,800–58,400 lbf
Total mass flow, $\dot{m}$	85–122 lbm/s	Vacuum I_{sp}	479–481 s
Chamber length, l_c	24 in.	Chamber pressure, P_0	2525–2710 psia
Outer chamber radius, r_{c_o}	6 in.	Chamber temperature, T_0	6770–6790 R
Inner chamber radius, r_{c_i}	2 in.	Throat area, A_t	7.8–10.4 in.^{2}
Expansion ratio, ϵ	125	Nozzle Length, l_n	14.5–14.8 in.
LOX bypass, %	90	Chamber volume, V_c	1560–1578 in.^{3}
LOX pump efficiency, $\eta_{p,\mathrm{LOX}}$	0.773	LOX temperatures, T_{LOX}	165–766 R
LOX turbine efficiency, $\eta_{t,\mathrm{LOX}}$	0.949	LOX Pressures, p_{LOX}	3650–4850 psia
LH2 pump 1 efficiency, $\eta_{p,\mathrm{LH2},1}$	0.8	Max LOX Mach number	0.35–0.39
LH2 pump 2 efficiency, $\eta_{p,\mathrm{LH2},2}$	0.83	LH2 temperatures, T_{LH2}	75–645 R
LH2 pump efficiency, $\eta_{p,\mathrm{LH2}}$	0.9	LH2 pressures, p_{LH2}	3850–5900 psia
		Max LH2 Mach number	0.87–0.91

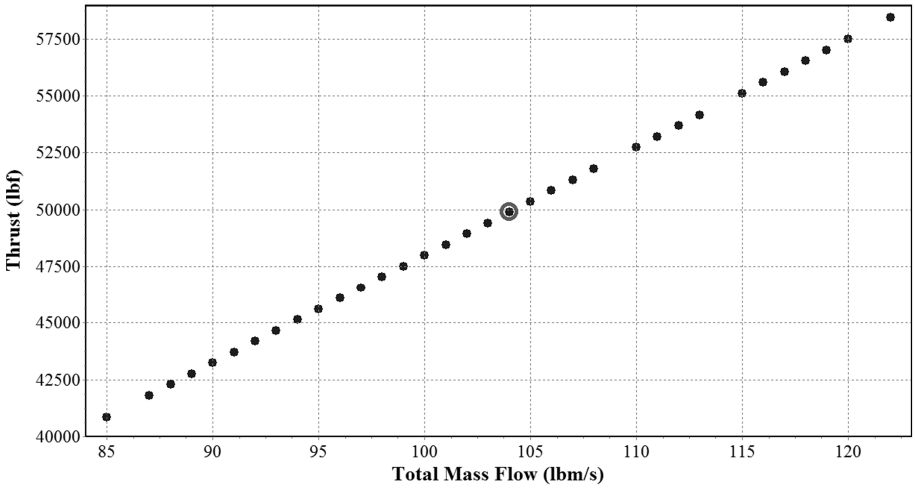

Fig. 17 Vacuum thrust vs total mass flow, system-level model.

Table 9 Parametric over chamber length

Design variables		Response variables	
O/F	7	Vacuum thrust, F_{vac}	57,100–58,200 lbf
Total mass flow, $\dot{m}$	121.25 lbm/s	Vacuum I_{sp}	471–480 s
Chamber length, l_c	14–26 in.	Chamber pressure, P_0	950–2975 psia
Outer chamber radius, r_{c_o}	6 in.	Chamber temperature, T_0	6435–6805 R
Inner chamber radius, r_{c_i}	2 in.	Throat area, A_t	9.8–28.9 in.^{2}
Expansion ratio, ϵ	125	Nozzle length, l_n	12.4–14.6 in.
LOX bypass, %	90	Chamber volume, V_c	1000–1700 in.^{3}
LOX pump efficiency, $\eta_{p,\mathrm{LOX}}$	0.773	LOX temperatures, T_{LOX}	160–780 R
LOX turbine efficiency, $\eta_{t,\mathrm{LOX}}$	0.949	LOX pressures, p_{LOX}	2300–5200 psia
LH2 pump 1 efficiency, $\eta_{p,\mathrm{LH2},1}$	0.8	Max LOX Mach number	0.32–0.42
LH2 pump 2 efficiency, $\eta_{p,\mathrm{LH2},2}$	0.83	LH2 temperatures, T_{LH2}	70–610 R
LH2 pump efficiency, $\eta_{p,\mathrm{LH2}}$	0.9	LH2 pressures, p_{LH2}	2450–6250 psia
		Max LH2 Mach number	0.86–0.97

to achieve 50,000 lbf thrust. Optimizing the DEAN design near 104 lbm/s will result in another weight savings over the original design.

Table 9 summarizes the final parametric study run on the DEAN system-level model, considering the chamber length from 14 to 26 in. The curve in Fig. 18 showing thrust versus chamber length has two transitions: one at 14.25 in. and one at 22.75 in. The shorter of these chamber lengths offers substantial weight savings while producing nearly the same thrust. This result supports selecting a chamber not longer than 14.25 in., but further optimization is warranted. Selecting a chamber length of 14.25 in. results in a total engine length of 27.85 in. The new length is nearly 25% shorter than the original design and 69% shorter than the RL10B-2 [9]. This result suggests that the DEAN architecture can be packaged in a considerably smaller volume than existing upper-stage engines.

B. Scaling the DEAN Engine

The previous parametric studies examined how three parameters, the O/F ratio, the total mass flow, and the chamber length, affect the weight and performance of the DEAN. Those three parameters will be the design variables to be modified in scaling the DEAN to the 50,000 lbf thrust target. The parametric studies suggest values for each of these parameters. As noted earlier, the engine provides the greatest I_{sp} at $O/F = 6$ for these parametric choices. Similarly, the study indicates a mass flow of approximately 104 lbm/s achieves the design vacuum thrust of 50,000 lbf. This result is for an engine operating at $O/F = 7$. With an O/F of six, the thrust will likely be higher. Finally, the results from the chamber length parametric study suggest a chamber length of 14.25 in. is an acceptable value. Entering these values into the system-level model results in a significantly smaller engine performing at 50,900 lbf thrust and 489 s I_{sp}. Table 10 summarizes this new design, and Fig. 19 shows this new, much smaller design next to the original design.

The performance values of this design are favorable. The 50,900 lbf thrust not only more closely matches the design requirements, but it also falls within the demonstrated 50,300 lbf of expander cycle engines, as seen in the upper-stage demonstrator engine [6]. The lengths of the engine chamber and nozzle are significantly smaller than the previous design, indicating the weight is similarly reduced. The converged values for the turbomachinery are equally promising. The power required by the pumps is properly balanced by power generated in the turbines; in the LOX cycle, this power is 40% of original design, while in the LH2 cycle, the power is only increased by 8% over the original design. Together with the reduced mass flows and the pressure ratios, the turbomachinery of the scaled DEAN design has both lighter and more robust options over the original design.

The results also indicate opportunities for improvement, both in areas where requirements are still exceeded by the design, including T/W, I_{sp}, and chamber pressure, and in areas where there are concerns including fluid Mach numbers and wall temperatures. The original design of the DEAN had an estimated weight of 479 lbm [1]. This gives an upper limit for the scaled DEAN T/W of 106, meeting or exceeding the required T/W. The vacuum I_{sp} is now over 5% higher than the requirement, suggesting the nozzle can be modified to save weight and meet the I_{sp} requirement. The chamber pressure is 25% lower than the previous design, which leads to a more robust chamber design. Turning to areas of concern, at least one constraint, the maximum LH2 Mach number, is still higher than desired. Additionally, the wall temperatures, which must stay within their material limits, still need to be determined. To determine the wall temperatures, notional materials need to be chosen.

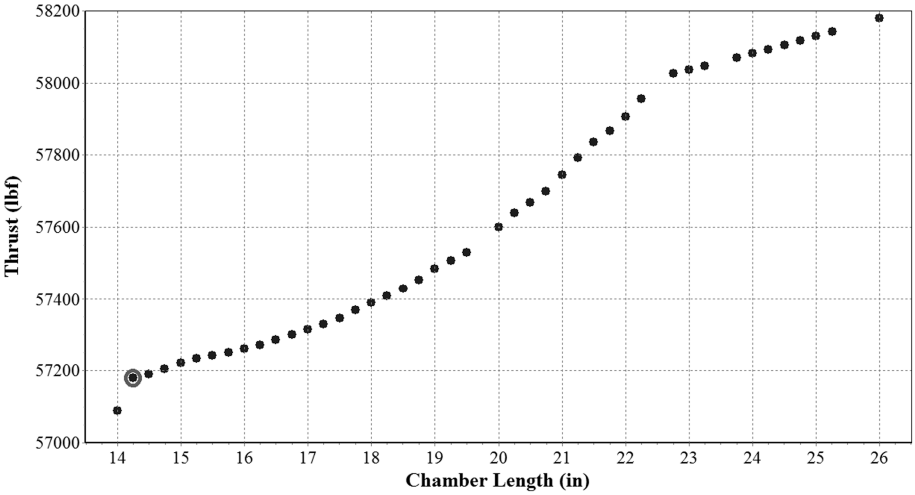

Fig. 18 Vacuum thrust vs chamber length, system-level model.

Table 10 Scaled DEAN design parameters

Design variables		Response variables	
O/F	6	Vacuum Thrust, F_{vac}	50,900 lbf
Total mass flow, $\dot{m}$	104 lbm/s	Vacuum I_{sp}	489 s
Chamber length, l_c	14.25 in.	Chamber pressure, P_0	1310 psia
Outer chamber radius, r_{c_o}	6 in.	Chamber temperature, T_0	6413 R
Inner chamber radius, r_{c_i}	2 in.	Throat area, A_t	18.9 in.^{2}
Expansion ratio, ϵ	125	Nozzle length, l_n	13.6 in.
LOX bypass, %	90	Chamber volume, V_c	970 in.^{3}
LOX pump efficiency, $\eta_{p,\mathrm{LOX}}$	0.773	LOX pump pressure ratio, $\mathrm{PR}_{p,\mathrm{LOX}}$	58
LOX turbine efficiency, $\eta_{t,\mathrm{LOX}}$	0.949	LOX pump power	1053 HP
LH2 pump 1 efficiency, $\eta_{p,\mathrm{LH2},1}$	0.8	LOX turbine pressure ratio, $\mathrm{PR}_{t,\mathrm{LOX}}$	1.6
LH2 pump 2 efficiency, $\eta_{p,\mathrm{LH2},2}$	0.83	LOX turbine power	1053 HP
LH2 pump efficiency, $\eta_{p,\mathrm{LH2}}$	0.9	LOX temperatures, T_{LOX}	160–435 R
		LOX pressures, p_{LOX}	2450–2600 psia
		Max LOX Mach number	0.37
		LH2 pumps pressure ratio, $\mathrm{PR}_{p,\mathrm{LH2}}$	9.3
		LH2 pump 1 power	417 HP
		LH2 pump 2 power	3430 HP
		LH2 turbine pressure ratio, $\mathrm{PR}_{t,\mathrm{LH2}}$	1.8
		LH2 turbine power	3847 HP
		LH2 temperaturess, T_{LH2}	73–324 R
		LH2 pressures, p_{LH2}	2960–3770 psia
		Max LH2 Mach number	0.96

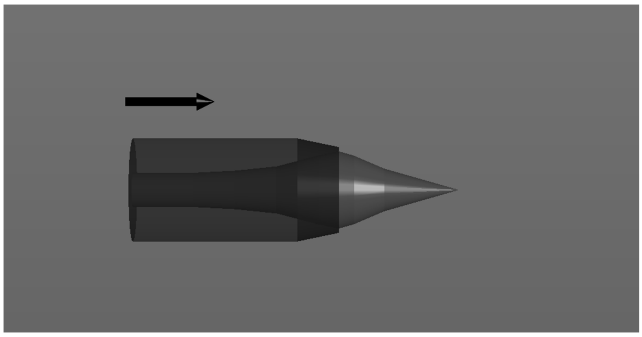

a) Original geometry for the DEAN

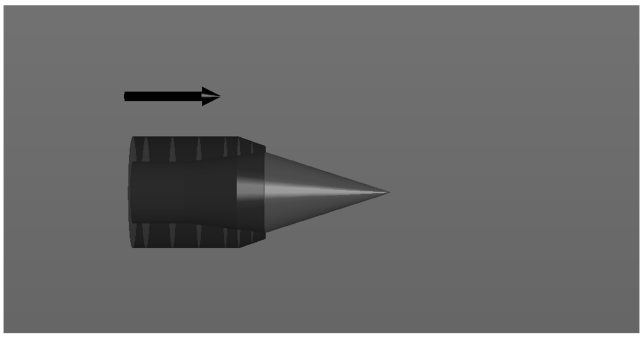

b) Geometry for the scaled DEAN

Fig. 19 Comparison of geometry for the scaled DEAN to the original geometry.

VI. Conclusions

The results of this study support two key conclusions. First, parametric modeling with automated trade studies is a powerful approach in conceptual design of rocket engines. Significant improvements were made to the design of the DEAN engine by modifying the numerical model to support parametric modeling and exploring the trade space through automated trade studies. These improvements included reducing the size of the turbomachinery by reducing the total mass flow, improving the oxidizer-to-fuel ratio for optimal thrust performance, and reducing the overall length by 25%. All of these savings were realized while maintaining the required vacuum thrust performance of 50,000 lbf and increasing the vacuum specific impulse from 472 to 489 s.

Second, the DEAN architecture offers significant performance gains over single-expander cycle-based upper-stage engines, such as the RL10B-2. The DEAN has a chamber pressure that is twice that of the RL10B-2. This increased chamber pressure results in twice the vacuum thrust and a 5% higher vacuum specific impulse. Finally, the DEAN engine is 69% shorter than the RL10B-2, despite its increased thrust and specific impulse.

Acknowledgments

The authors would like to thank the following institutions for providing the software used in this research: NASA for the Numerical Propulsion System Simulation package and Phoenix Integration for providing ModelCenter. The views expressed in this paper are those of the authors and do not reflect the official policy or position of the U.S. Air Force, the U.S. Department of Defense, or the U.S. Government.

References

[1] Martin, D. F., "Computational Design of Upperstage Chamber, Aerospike, and Cooling Jacket of Dual-Expander Rocket Engine," M.S. Thesis, Air Force Inst. of Technology, Wright-Patterson, AFB, OH, 2008.

[2] Minick, A., and Peery, S., "Design and Development of an Advanced Liquid Hydrogen Turbopump." 34th AIAA/ASME/SAE/ASEE Joint Propulsion Conference and Exhibit, Cleveland, OH, AIAA, Paper 1998-3681, 13–15 July 1998.

[3] Humble, R. W., *Space Propulsion Analysis and Design*, McGraw–Hill, New York, 1995.

[4] Strain, W. S., "Design of an Oxygen Turbopump for a Dual Expander Cycle Rocket Engine," M.S. Thesis, Air Force Inst. of Technology, Wright-Patterson, AFB, OH, 2008.

[5] "NPSS User Guide," Ver. 5, NASA Glenn Research Center, Cleveland, OH, 30 May 2006.

[6] Arguello, A. A., "The Concept Design of a Split Flow Liquid Hydrogen Turbopump," M.S. Thesis, Air Force Inst. of Technology, Wright-Patterson, AFB, OH, 2008.

[7] *ModelCenter 9.0 User Manual*, Phoenix Integration, Blacksburg, VA, 2010.

[8] Krach, A. E., and Sutton, A. M., "Another Look at the Practical and Theoretical Limits of an Expander Cycle, LOX/H2 Engine," 35th AIAA/ASME/SAE/ASEE Joint Propulsion Conference and Exhibit, Los Angeles, AIAA Paper 1999-2473, 20–24 June 1999.

[9] Sutton, G. P., *Rocket Propulsion Elements*, 8th ed., Wiley, Hoboken, NJ, 2010.

J. Martin
Associate Editor